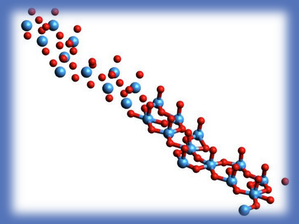

Probing Atomic Structure of Tantala Coatings with EXAFS

Franklin Liou (fliou@stanford.edu)

E. L. Ginzton Laboratory, Stanford University, Stanford CA 94305

ABSTRACT

We perform Extended X-ray Absorption Fine Structure (EXAFS) analysis on Ion-Beam Sputtered (IBS) amorphous tantala-based coatings for use in gravitational wave detectors. Nearest neighbor distances and distributions were determined by EXAFS analysis. We found that the Ta atom in amorphous tantala and titania doped (Ti-doped) tantala are surrounded by 4 shells of atoms in sequence; oxygen, metal, oxygen and metal. We investigate the effects of different annealing temperatures and Ti-doping concentrations on the structure of tantala. While annealing temperature has only a subtle effect on the short-range structure of pure tantala, increasing annealing temperature in Ti-doped tantala increases the Ti/Ta ratio in the second shell. All Ti-doped tantala show a deficiency in Ti sites, suggesting inhomogeneity of atomic species. The introduction of Ti in tantala mainly changes second and third shell structure. Finally, we observe crystallization in 75% Ti-doped tantala coating.

MOTIVATION

A key limitation to the sensitivity of LIGO is the thermal noise, which is directly related to the mechanical loss arising in the mirror coatings. A common coating material is amorphous tantala (Ta_2O_5). Recent work on this material suggests that changes in short-range structure strongly correlate with mechanical loss[10]. To better resolve such structural changes, we use EXAFS to probe radial atomic distances from tantalum. Although amorphous materials do not exhibit long-range order characteristic of crystals, specific fragments with short-range order are still commonly found throughout the material, making EXAFS a useful tool for probing short-range structure (≤ 10Å). Our aim is to correlate the short-range structure with mechanical loss to better understand mechanical loss mechanisms in amorphous coatings.

BACKGROUND

Literature on the structure of crystal tantala indicates several different forms with distinct spacegroups. Furthermore, literature on the same form of tantala disagree on its structure, with typical unit cells ranging from 5 to 40 Å in length. This suggests that crystalline tantala is polymorphous and not well understood. However, judging from similarities in different models, we observe alternating oxygen and tantalum shells.

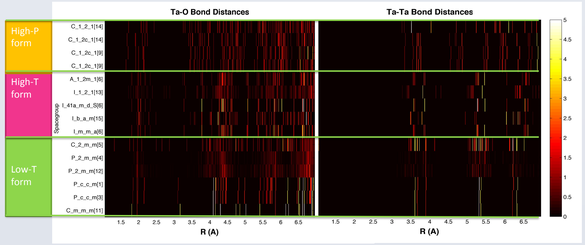

Fig 1. Ta-O and Ta-Ta Bond Distances of Several Crystalline Tantala Models [1-6,9,11-15]

EXAFS

EXAFS uses the scattering states of a photoelectron from a central atom to gather information on scattering atoms (scatterers) around it. The total cross-section of the photoelectron is a function of wavenumber k. Since fluorescence from the sample is proportional to the photoelectron cross-section, we can measure a dimensionless quantity χ(k), which is the intensity of fluorescent X-rays normalized to the intensity of incoming X-rays, filtering out low-frequency components. The theoretical form of χ(k) is calculated with the EXAFS equation, with several fitting parameters:

$$\chi(k) = \sum_i \frac{N_i S_0^2 f_i(k)}{k R_i^2} e^{-2R_i/\lambda(k)} e^{-2k^2\sigma_i^2} \sin(2kR_i + \delta_i(k))$$

The terms f(k), λ(k) and δ(k) are calculated using scattering theory with FEFF8[2]. The fitting parameters are $N_i S_0^2$, the scattering amplitude (proportional to the number of scatterers of same type); R_i, the distance to the scatterer; σ^2, the Mean Square Relative Displacement (a measure of atomic thermal vibration); and E_0, the Absorption Energy.

METHODS

The samples in our study are single-layer 500 nm-thick IBS tantala coatings on silica substrates manufactured by CSIRO. The samples we studied have Ti-doping concentrations of 0%, 25%, 55% and 75%. The samples were also annealed for 24 hours in air at different temperatures, 300ºC and 600ºC, and also unannealed samples.

EXAFS spectra were taken at the Stanford Synchrotron Radiation Lightsource (SSRL). We analyzed the fluorescent spectra of the tantalum L_{III} absorption edge to obtain χ(k), which was subsequently fitted with multiple single-scatterer spectra calculated by FEFF8[2], using IFEFFIT[8] as the fitting engine.

RESULTS

The Fourier Transform of χ(k) spectra, χ(R), is a representation of nearest neighbor distributions. The χ(R) for all of the samples are plotted in Fig 2. The peaks are usually shifted by 0.3-0.4 Å to lower-R values due to a phase shift of the electron wavefunction in the scattering process.

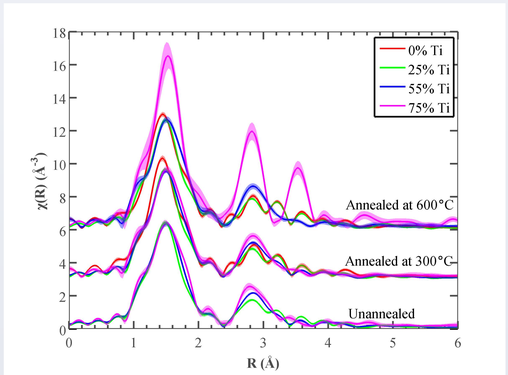

Fig 2. χ(R) Spectra of all Samples

The fits to the pure tantala samples (Figs 3,4; Tables 1,2) indicate 4 shells of atoms consisting of oxygen in the first shell, Ta in the second shell, oxygen in the third shell and Ta in the fourth shell. The first shell contains two oxygen at different distances to the central Ta.

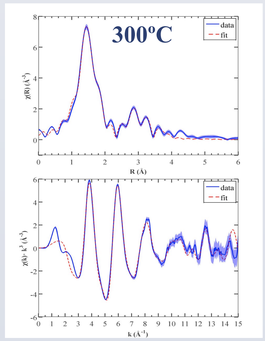

Fig 3. χ(R) of Pure Tantala Annealed at 300ºC and Fits (top). Corresponding χ(k) (bottom).

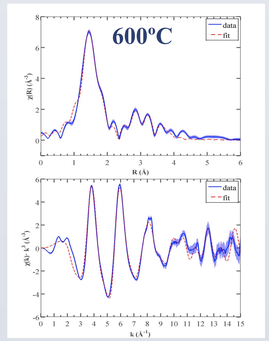

Fig 4. χ(R) of Pure Tantala Annealed at 600ºC and Fits (top). Corresponding χ(k) (bottom).

Table 1. Fitting parameters of Pure Tantala Annealed at 300ºC

Scatterer	R	σ^2	NS_0^2	$N(S_0^2=0.8)$
Ta-O	1.85(4)	0.0024(27)	1.52(172*)	1.90(216)
Ta-O	1.99(6)	0.0058(57)	2.48(178*)	3.11(223)
Ta-Ta	3.14(2)	0.0075(25)	1.14(61)	1.42(76)
Ta-O	3.55(2)	0.0024(24)	1.98(57)	2.47(72)
Ta-Ta	3.88(3)	0.0066(68)	0.41(58)	0.52(73)
		Fitted E_0	-3.426	± 0.792
		*Total first shell NS_0^2	4.00	±0.217

Table 2. Fitting parameters of Pure Tantala Annealed at 600ºC

Scatterer	R	σ^2	NS_0^2	$N(S_0^2=0.8)$
Ta-O	1.84(8)	0.0021(60)	1.26(350*)	1.57(437)
Ta-O	1.98(12)	0.0063(122)	2.54(369*)	3.18(461)
Ta-Ta	3.14(4)	0.0077(52)	1.11(115)	1.39(143)
Ta-O	3.55(3)	0.0011(34)	1.82(90)	2.27(113)
Ta-Ta	3.89(4)	0.0069(84)	0.65(109)	0.81(137)
		Fitted E_0	-3.628	± 1.441
		*Total first shell NS_0^2	3.80	±0.386

Effect of Different Annealing Temperatures

Different annealing temperatures only have a subtle effect on the short-range order of pure tantala samples. The distances and amplitudes of the contributing scatterers are plotted in Fig 6.

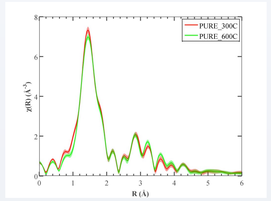

Fig 5. χ(R) of Pure Tantala Samples

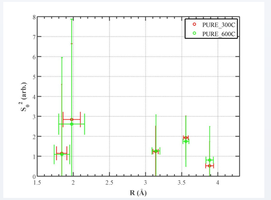

Fig 6. Fitted Distances and Amplitudes of Scatterers to χ(R) of Pure Tantala

For 25% Ti-doped tantala, the peak at 3.1 Å increases in amplitude with temperature. Fits indicate that the feature is due to changing Ti/Ta ratio in the second shell.

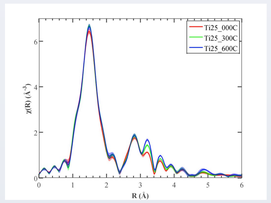

Fig 7. χ(R) of 25% Ti-doped Tantala Samples

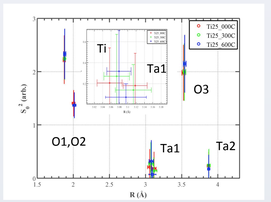

Fig 8. Fitted Distances and Amplitudes of Scatterers to χ(R) of 25% Ti-doped Tantala

In 55% Ti-doped tantala, changes are also seen in the second shell. However, the sample annealed at 600ºC exhibits different behavior in the second shell tantalum and third shell (oxygen).

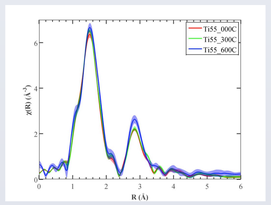

Fig 9. χ(R) of 55% Ti-doped Tantala Samples

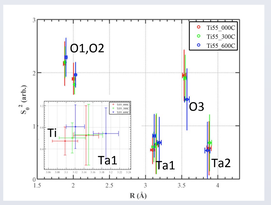

Fig 10. Fitted Distances and Amplitudes of Scatterers to χ(R) of 55% Ti-doped Tantala

Effect of Ti-Doping

Ti-doping amorphous tantala mainly affects nearest neighbor distributions in the second and third shell. We observe that the Ti scatterer amplitudes are roughly the same through all Ti-doped tantala samples, indicating that Ti does not replace the Ta in the second shell as we add Ti in tantala. We also observe much less Ti in the second shell than expected from stoichiometry, which may be due to inhomogeneity of tantalum and titanium regions. The amplitude of scattering from the third shell oxygen decreases as more Ti is added.

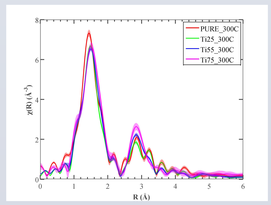

Fig 11. χ(R) of Tantala Samples Annealed at 300ºC

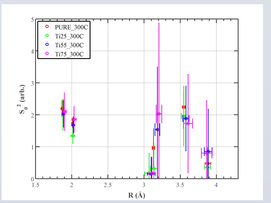

Fig 12. Fitted Distances and Amplitudes of Scatterers to χ(R) of Tantala Samples Annealed at 300ºC

Crystallization

75% Ti-doped tantala annealed at 600ºC exhibits crystallization, with atomic shells now consisting of oxygen in the first shell, Ti in the second shell and a mixture of Ta and Ti in the third shell. The number of surrounding oxygens is significantly larger than that of the amorphous samples and agrees with oxygen coordination obtained from a previous NMR study[7].

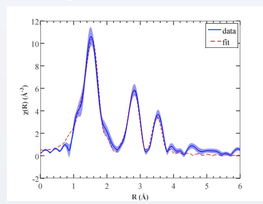

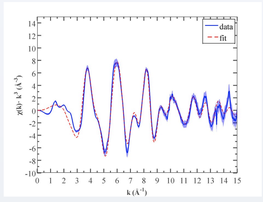

Fig 3. χ(R) of 75% Ti-doped Tantala Annealed at 600ºC and Fits (left). Corresponding χ(k) (right).

Table 3. Fitting parameters of 75% Ti-doped Tantala Annealed at 600ºC

Scatterer	R	σ^2	NS_0^2	$N(S_0^2=0.8)$
Ta-O	1.94(1)	0.0080(11)	5.06(51)	6.33(63)
Ta-Ti	3.13(2)	0.0071(30)	2.22(109)	2.77(136)
Ta-Ta	3.12(4)	0.0167(62)	6.20(370)	7.75(463)
Ta-Ti	3.87(1)	0.0016(25)	0.98(49)	1.22(61)
		Fitted E_0	-1.795	±1.071

CONCLUSIONS

Although amorphous materials do not have long-range order, there is still enough short-range order to resolve spectral features < 4 Å with EXAFS. The 4 shell single-scatterer structure provides a good model for amorphous tantala glass:

Shells	R (Å)	Occupancy
O1, O2	1.85, 1.95	4—5
Ti1, Ta1	3.1, 3.15	0.4—0.5, 1—1.4
O3	3.6	2.4—3
Ta2	3.9	0.5—1

Since the occupancy of Ti is much lower than expected, we conclude that Ti does not replace Ta in tantala in the short range. The structure of pure tantala remains stable with annealing temperature. However, Ti/Ta ratio increases in Ti-doped samples as annealing temperature is raised, suggesting that annealing homogenizes the two species. This tendency manifests itself in the crystallization of the 75% Ti sample annealed at 600ºC, which has the highest Ti concentration and highest annealing temperature in all our samples.

Future work will use our EXAFS data to build 3-D models of amorphous tantala with Reverse Monte-Carlo Simulation, and also correlate our observed changes in the atomic structure with mechanical loss.

REFERENCES

1. Aleshina, L.A.; Loginova, S.V., Kristallografiya (2002) 47, (3) p460-p464
2. Ankudinov, A.L., et al., *Physical Review B* 58.12 (1998), p7565
3. Demont, A.; et al., Chemistry - A European Journal (2013) 19, (38) p12711-p12719
4. Hummel, H.U.; Fackler, et al.,R. Chemische Berichte (1992) 125, p551-p556
5. Lehovec, K., Journal of the Less-Common Metals (1964) 7, p397-p410
6. Liu, X.-Q.; et al., Acta Materialia. (2007) 55, p2385-p2396
7. Kim, N.; Stebbins, J.,Journal of Non-Crystalline Solids, (2013) 378, p158-162
8. Newville, M., *Journal of synchrotron radiation* 8.2 (2001): 322-324
9. Perez-Walton, S.; et al., Physica Status Solidi B - Basic Solid State Physics (2013) 250, (8) p1644-p1650
10. Bassiri, R.; et al., Acta Materialia, (2013) 61, (4), p1070-1077
11. Schmid, S.; Fung, V. m, Australian Journal of Chemistry (2012) 65, p851-p859
12. Stephenson, N.C.; Roth, R.S., Acta Crystallographica B (24,1968-38,1982) (1971) 27, p1037-p1044
13. Stephenson, N.C.; Roth, R.S., Journal of Solid State Chemistry (1971) 3, p145-p153
14. Zibrov, I.P.; Filonenko; et al., Acta Crystallographica, Section B: Structural Science (2000) 56, p659-p665
15. Zibrov, I.P.; Filonenko; et al., Zhurnal Neorganicheskoi Khimii (2003) 48, p543-p550

ACKNOWLEDGEMENTS

The LIGO DCC document number of this poster is LIGO-G1400977

This research was funded by NSF grant PHY-1068596

I would like to thank Dr. Riccardo Bassiri, Dr. Apurva Mehta, Dr. Badri Shyam, Prof. Martin Fejer and my colleagues in the LSC for their support and guidance.